C. R. Chimie 20 (2017) 1072–1082

Contents lists available at ScienceDirect

Comptes Rendus Chimie

www.sciencedirect.com

Full paper/Mémoire

Antioxidant properties of several caffeic acid derivatives: A theoretical study

Alicja Urbaniak [a], Jacek Kujawski [b], Kornelia Czaja [b], Malgorzata Szelag [c, *]

[a] Department of Bioorganic Chemistry, Faculty of Chemistry, Adam Mickiewicz University, Umultowska 89b, 61-614 Poznań, Poland
[b] Department of Organic Chemistry, Faculty of Pharmacy, Poznan University of Medical Sciences, Grunwaldzka 6, 60-780 Poznań, Poland
[c] Department of Human Molecular Genetics, Faculty of Biology, Adam Mickiewicz University, Umultowska 89, 61-614 Poznań, Poland

ARTICLE INFO

Article history:
Received 11 June 2017
Accepted 22 August 2017
Available online 29 September 2017

Keywords:
Computational chemistry
Quantum chemical calculation
Radical
Caffeic acid
Polyphenol
M05-2X

ABSTRACT

Phenolic acids constitute a family of natural compounds that can be found in a wide variety of plants and food. Among them only ferulic, *p*-coumaric, chlorogenic, and caffeic acids were recently investigated. There are no data about antioxidant activity of single molecules of fertaric, coutaric, caftaric, dactylifric, and neochlorogenic acids and prenyl caffeate. In a continuation of our attempts to clarify their antioxidant activity, we present herein *in silico* studies concerning four mechanisms of interaction of phenolic antioxidants with free radicals: hydrogen atom transfer (HAT), (sequential proton loss electron transfer (SPLET), single electron transfer followed by proton transfer, and transition metals chelation, determining several parameters such as bond dissociation enthalpy; proton affinity; adiabatic ionization potential; highest occupied molecular orbital, lowest unoccupied molecular orbital, singly occupied molecular orbital; spin density; stabilization energy (ΔE_{ISO}); deprotonation enthalpy/energy ($\Delta H_{acidity}$ and $\Delta G_{acidity}$); and second-order perturbation energy $E(2)$. We have proved that for all studied compounds the HAT mechanism was preferred in vacuum as well as in benzene and amyl acetate solvent media, whereas SPLET approach was significantly exposed especially in water. The most active antioxidants (according to the HAT approach) were compounds prenyl caffeate, methyl caffeate, and caffeic acid phenethyl ester, whereas the activity of *trans* and *cis* isomers of chicoric derivatives was related to the SPLET protocol. We also observed that *trans* isomers of caffeic, ferulic, and *p*-coumaric derivatives were not enough effective in all environments, when compared with other studied molecules. Moreover, we have noticed that the *ortho* position of the phenylic ring influenced profitably on antioxidant activity in all analyzed compounds.

1. Introduction

Cellular injury in the form of damaged DNA, lipids, and proteins is mostly caused by reactive oxygen species (ROS), namely, hydroxyls ($HO^{\bullet}$), superoxides ($O_2^{\bullet -}$), peroxyls ($ROO^{\bullet}$), alkoxyls ($RO^{\bullet}$), and nitric oxides ($NO^{\bullet}$). Therefore, the excess of ROS can be immediately eliminated in the cell by various cellular antioxidant enzymes and redox molecules [1]. Moreover, many natural and synthetic antioxidants can protect cells against ROS due to their free radical scavenging activity. For this reason, there is a huge interest in searching for novel compounds exhibiting this ability. A group of caffeic acid secondary metabolites, derived from plants, is one of the most studied. Their function is inter alia to protect against UV radiation and pathogen aggression [2], as proven in many in vitro and in vivo studies [2–6], to name a few.

* Corresponding author.
E-mail address: grete@amu.edu.pl (M. Szelag).

http://dx.doi.org/10.1016/j.crci.2017.08.003
1631-0748/

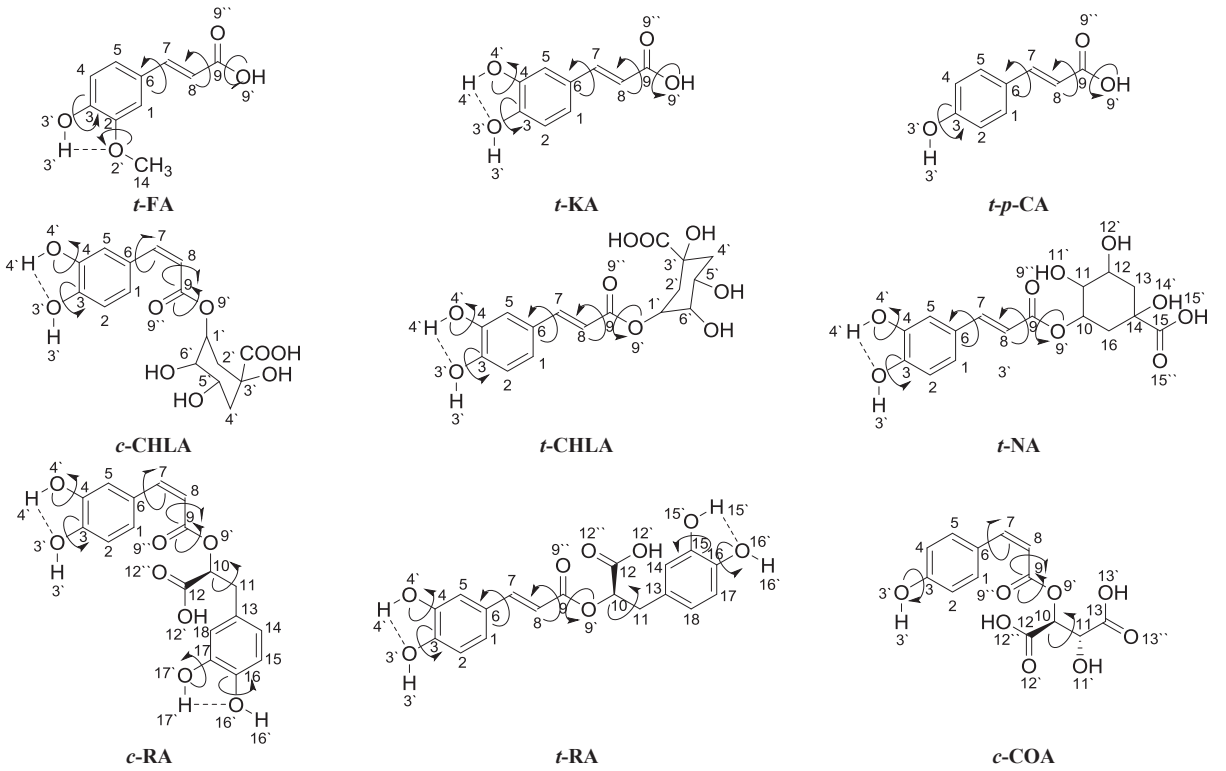

Fig. 1. Schematic representation of the most stable calculated conformers. Rotations were involved in geometry optimization. The atom numbering and internal hydrogen bonds are also included.

Although ferulic, *p*-coumaric, chlorogenic, and caffeic acids were studied in depth [2–6], there are no data about antioxidant activity of fertaric, coutaric, caftaric, dactylifric, and neochlorogenic acids and prenyl caffeate (PC). These compounds were only tested as components of more complex extracts but the activity of individual molecules seems to be unknown [7–10]. Therefore, on this account the presented study is the first attempt to investigate their antioxidant activity using *in silico* techniques.

Seeds and sprouts of legume plants are a rich source of phenolic acids. Because of their nutritive properties, they are considered as functional food. In food industry, phenolics may affect inter alia the oxidative stability of products. Because of their ability to prevent diseases associated with oxidative stress they are interesting for consumers and producers [11]. Peanut sprouts (*Arachis hypogaea* L.) constitute a large source of phenolic acids. Significant accumulation of caffeic acid is observed at an early stage of their growth. It was also observed that after purification caffeic acid showed a strong intracellular antioxidant ability in human erythrocytes [12]. In turn, the main antioxidant in extract from Teaw leaves (*Cratoxylum formosum* Dyer) was chlorogenic acid. Fresh leaves taken from *C. formosum* Dyer are being used as traditional food in Thailand [13]. Several bioassays confirmed that chlorogenic acid seems to be a major to the antioxidant activity and thus may be regarded as a significant source of natural antioxidant [14].

There are four mechanisms described in the literature used for assessment of phenolic antioxidant interactions with free radicals [15,16]: hydrogen atom transfer (HAT) [17,18], sequential proton loss electron transfer (SPLET) [19,20], single electron transfer followed by proton transfer (SET-PT) [17,21], and transition metals chelation (TMC) [17,22]. The other important parameters related to antioxidant activity are highest occupied molecular orbital (HOMO), lowest unoccupied molecular orbital (LUMO), canonical singly occupied molecular orbital (SOMO) distributions, and spin density (SD). Low values of HOMO energy are related to weak proton donation abilities and indicate the parts of the molecule, which are susceptible to free radical attack [16]. It is well known that the difference between LUMO and HOMO energies provides information about chemical activity of the molecule [23]. The SOMO parameter, however, is associated with the distribution of nonpaired electron and SD factor and provides information about free radical stability.

Despite the fact that *p*-coumaric, caffeic, and ferulic acids were recently carefully theoretically studied (Supplementary Table 1), we decided to carry out calculations using global-hybrid *meta*-GGA (generalized gradient approximation) functional, such as the M05-2X [24]. This procedure allowed us to compare results obtained for novel caffeic acid derivatives with others similar compounds with the same core and/or comparable activity. Nevertheless, *trans*-rosmarinic, chlorogenic acids, and phenethyl ester have been recently described, but authors of cited

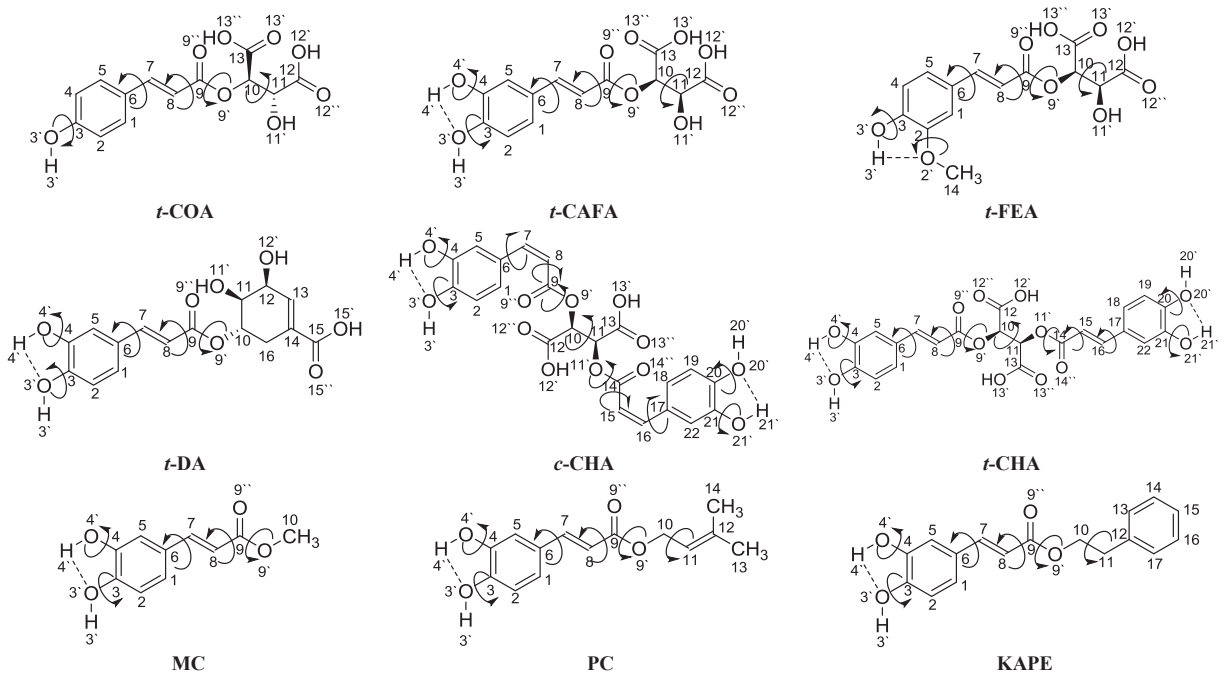

Fig. 1. (*Continued*).

reports focused attention only on basic assessment of activity (Supplementary Table 1) [25–29]. Thus, we decided to fill this gap of data with the missing antioxidant descriptors as they are important for the understanding of free radical scavenging activity of the molecules. The up to date *in silico* antioxidant studies on phenolic acids are depicted in Supplementary Table 1. Furthermore, no attention has been paid to determine antioxidant descriptors for more complex caffeic acid derivatives, namely, chicoric, coutaric, caftaric, fertaric, dactylifric, and neochlorogenic acids, PC, and methyl caffeate (MC). Lack of both experimental and theoretical data for listed compounds prompted us to perform following investigations.

In this study, we provide a full theoretical analysis of structure–antioxidant activity relationship for caffeic acid derivatives being available in the Human Metabolome Database (http://www.hmdb.ca): both *cis* and *trans* isomers of chicoric (*c*-CHA, *t*-CHA), chlorogenic (*c*-CHLA, *t*-CHLA), coutaric (*c*-COA and *t*-COA), and rosmarinic acids (*c*-RA and *t*-RA), *trans* isomers of ferulic (*t*-FA), caffeic (*t*-KA), *p*-coumaric (*t*-*p*-CA), caftaric (*t*-CAFA), fertaric (*t*-FEA), dactylifric (*t*-DA), neochlorogenic acids (*t*-NA), MC, caffeic acid phenethyl ester (KAPE), and PC.

The main goal of our study was to determine *in silico* parameters related to molecules' antioxidant activity, namely, bond dissociation enthalpy (BDE), proton affinity (PA), adiabatic ionization potential (AIP), HOMO, LUMO, SOMO, SD, stabilization energy (ΔE_{ISO}), deprotonation enthalpy/energy ($\Delta H_{acidity}$ and $\Delta G_{acidity}$), and second-order perturbation energy $E(2)$, to compare antioxidant potential of investigated compounds and to determine mechanism preferred for this class of molecules.

2. Computational details

All calculations presented in this work were performed with the Gaussian 09B.01W [40]. The molecules were submitted to geometry conformational search at HF/6-31G(d,p) level of theory. Dihedral angles $\alpha = C_5–C_6–C_7–C_8$ (rotation of the benzene ring around the $C_6–C_7$ single bond) and $\beta = C_7–C_8–C_9–O_{9'}$ (rotation of the carboxyl group around the $C_8–C_9$ single bond) were scanned to construct the potential energy surface scans. Moreover, the rotation of hydroxyl and methoxyl groups related to $C_Y–O_{Y'}$ bonds and other structurally significant groups were also analyzed (Fig. 1). Geometries in their energy minima were further fully optimized in their ground states (no negative frequencies in the generated IR spectrum were detected during optimization) in vacuum using the Berny algorithm and tight convergence in the SCF (self-consistent field) using DFT (density functional theory) method with M05-2X functional [24,41] and 6-311++G(d,p) basis set. For neutral, anionic, and dianionic forms we applied the restricted level of theory, whereas we applied the unrestricted level of theory for radicals and cation radicals. The provided electronic geometries determined the approximate position of the energy minimum structures. Calculations performed in solvation media were accomplished according to the same methodology using SMD (solvent model density) model [42] with dielectric constant (ε) for water ($\varepsilon = 78.3553$), benzene ($\varepsilon = 2.2706$), and amyl acetate ($\varepsilon = 4.7297$). For calculation of second-order perturbation energies $E(2)$, we have applied the natural bond orbital (NBO) analysis as implemented in *Gaussian* software [40]. The HOMO, LUMO, SOMO, and SD distributions related to the electron-

donating properties were determined in vacuum, water, benzene, and amyl acetate media at the M05-2X/6-311++G(d,p) level of theory. In our study, we determined the following descriptors associated with the free radical scavenging properties of investigated compounds:

HAT mechanism

$$BDE_H = H^{\bullet}_{ArO} + H^{\bullet}_{H} - H_{ArOH} \quad (2.1)$$

$$BDE_G = G^{\bullet}_{ArO} + G^{\bullet}_{H} - G_{ArOH} \quad (2.2)$$

SPLET mechanism

$$PA_H = H^{-}_{ArO} + H^{+}_{H} - H_{ArOH} \quad (2.3)$$

$$PA_G = G^{-}_{ArO} + G^{+}_{H} - G_{ArOH} \quad (2.4)$$

SET-PT mechanism

$$AIP_H = H^{\bullet+}_{AroH} - H_{ArOH} + H_e \quad (2.5)$$

$$AIP_G = G^{\bullet+}_{AroH} - G_{ArOH} + G_e \quad (2.6)$$

TMC mechanism

$$\Delta H_{acidity} = H^{-}_{ArO} - H_{ArOH} \quad (2.7)$$

$$\Delta G_{acidity} = G^{-}_{ArO} - G_{ArOH} \quad (2.8)$$

Energy of stabilization

$$\Delta E_{ISO} = (E^{\bullet}_{ArO} + E_{DPPHH}) - (E_{ArOH} + E_{DPPH}) \quad (2.9)$$

$$\Delta E_{ISO} = (E^{\bullet}_{ArO} + E_{PhOH}) - (E_{ArOH} + E^{\bullet}_{PhO}) \quad (2.10)$$

where $H_{ArOH/ArO^-/ArO^{\bullet}/ArOH^{\bullet+}}$ is the enthalpy of compound, anion, radical, or cation radical; $H_{H^{\bullet}/H^+/e}$ is the enthalpy of H atom, proton, or electron; $G_{ArOH/ArO^-/ArO^{\bullet}/ArOH^{\bullet+}}$ is the Gibbs free energy of compound, anion, radical, or cation radical; $G_{H^{\bullet}/H^+/e}$ is the Gibbs free energy of H atom, proton, or electron; E_{ArOH} is the energy of compound; $E_{ArO^{\bullet}}$ is the energy of radical; E_{PhOH} is the energy of phenol; $E_{PhO^{\bullet}}$ is the energy of phenol radical; and $E_{DPPH/DPPHH}$ is the energy of DPPH (2,2-diphenyl-1-picrylhydrazyl) radical and the non-radical form.

Experimental and theoretical enthalpy and Gibbs free energy values for $H^{\bullet}$, H^+, and electron applied in calculations have been gathered in Supplementary Table 2 [21,43,44]. The enthalpy and Gibbs free energy values in media have been calculated by addition of the solvation correction ($\Delta_{solv}H$) to the enthalpy or Gibbs free energy of the particle (H^+, $H^{\bullet}$, e^-) in vacuum [21,43–45], according to the following Eqs. 2.11–2.16:

$$H(H^+)_{solv} = H(H^+)_{vacuum} \Delta_{solv}H(H^+) \quad (2.11)$$

$$G(H^+)_{solv} = G(H^+)_{vacuum} + \Delta_{solv}G(H^+) \quad (2.12)$$

$$H(H^{\bullet})_{solv} = H(H^{\bullet})_{vacuum} + \Delta_{solv}H(H^{\bullet}) \quad (2.13)$$

$$G(H^{\bullet})_{solv} = G(H^{\bullet})_{vacuum} + \Delta_{solv}G(H^{\bullet}) \quad (2.14)$$

$$H(e^-)_{solv} = H(e^-)_{vacuum} + \Delta_{solv}H(e^-) \quad (2.15)$$

$$G(e^-)_{solv} = G(e^-)_{vacuum} + \Delta_{solv}G(e^-) \quad (2.16)$$

3. Results and discussion

3.1. Geometry optimization

To explain the link between the molecular structure and antioxidant activity of caffeic acid and related polyphenols we focused our attention on their conformational and electronic features. Full geometry optimization was performed for all the studied molecules in vacuum, water, benzene, and amyl acetate media (SMD solvation model). Geometries of neutral, monoanionic, and dianionic radical and cation radical forms were found in their energy minima, these structures were calculated at the M05-2X/6-311++G(d,p) level of theory. To understand the effect of conformational and rotational changes on the molecule stability we studied several significant structural parameters: (1) rotation around C_6–C_7 and C_8–C_9 bonds (for all compounds), and respective, symmetric C_{14}–C_{15} and C_{16}–C_{17} bonds for *c*-CHA and *t*-CHA; (2) *syn* and *anti* geometries represented by C_7–C_8–C_9–$O_{9'}$ dihedral angle equal to 0° or 180°, respectively (for all compounds); (3) orientation of $H_{9'}$ atom relative to the carbonyl group, resulting in *s-cis* or *s-trans* conformation (for acidic analytes); (4) orientation of the characteristic for the compounds hydroxyl and methoxyl ring substituents, determined by rotation of the respective C–O bonds; (5) rotation around C_{10}–C_{11} bond for *c*-RA, *t*-RA, *c*-COA, *t*-COA, *t*-CAFA, *t*-FEA, *c*-CHA, *t*-CHA, PC, and KAPE derivatives; and (6) rotation around $O_{11'}$–C_{14} bond for *c*-CHA and *t*-CHA compounds. For further studies, we used geometries of the optimized rotamers (Fig. 1).

It turned out that the most stable rotamers contained vinyl bond and carboxylic moiety (within *t*-FA, *t*-KA, and *t*-*p*-CA derivatives) and were coplanar to the aromatic ring. This assumption was confirmed by 0° value of dihedral angles related to the rotation around C_6–C_7 and C_8–C_9 bonds for all the studied molecules. Furthermore, because of the π–electron delocalization among the aromatic ring, vinyl bond, and carboxylic moiety these bonds are partially double. In most cases, detected small changes in the O–H bond length (from 0.96 to 0.97 Å *in vacuo* or polar media, respectively) were almost identical for all the studied compounds. No other significant dependences have been noticed.

The most favorable conformation of hydroxyl and methoxyl groups was given by their coplanar location to the aromatic ring (Fig. 1 and Supplementary Fig. 1), which was indicated by 0° value of dihedral angles: C_X–C_Y–$O_{Y'}$–$H_{Y'}$ and C_X–C_Y–$O_{Y'}$–C_Z. For NA, RA, CAFA, DA, MC, EC, PC, and KAPE derivatives, O–H moiety allowed the formation of a stabilizing intramolecular types of interactions: (O)$H_{4'}\cdots O_{3'}$(H) and additionally (O)$H_{17'}\cdots O_{16'}$(H) for *c*-RA, (O)$H_{15'}\cdots O_{16'}$(H) for *t*-RA, (O)$H_{21'}\cdots O_{20'}$(H) for CHA, whereas

Table 1
Analysis of the interaction between electron donor and acceptor orbitals (hydrogen bonding) calculated with M05-2X/6-311++G(d,p) level of theory.

Donor-acceptor	Vacuum	Water	Benzene	Amyl acetate
	E(2) (kcal/mol)	*E*(2) (kcal/mol)	*E*(2) (kcal/mol)	*E*(2) (kcal/mol)
t-KA LP (1) O3′ → σ* O4′H4′	1.18	0.80	1.04	1.03
c-CHLA LP (1) O3′ → σ* O4′H4′	183.29	0.80	5.06	3.79
t-CHLA LP (1) O3′ → σ* O4′H4′	160.68	5.27	5.88	5.68
t-NA LP (1) O3′ → σ* O4′H4′	1.02	0.78	1.03	1.03
c-RA LP (1) O3′ → σ* O4′H4′	0.73	0.86	1.45	1.03
c-RA LP (1) O16′ → σ* O17′H17′	n/a	0.84	n/a	1.08
t-RA LP (1) O3′ → σ* O4′H4′	n/a	0.93	n/a	n/a
t-RA LP (1) O16′ → σ* O15′H15′	1.09	0.80	1.10	1.09
t-CAFA LP (1) O3′ → σ* O4′H4′	1.01	0.78	1.03	1.02
t-DA LP (1) O3′ → σ* O4′H4′	1.01	0.79	1.02	1.02
c-CHA LP (1) O3′ → σ* O4′H4′	1.17	0.76	1.15	1.09
c-CHA LP (1) O20′ → σ* O21′H21′	1.39	0.99	1.40	1.33
t-CHA LP (1) O3′ → σ* O4′H4′	n/a	n/a	n/a	n/a
t-CHA LP (1) O20′ → σ* O21′H21′	1.01	0.77	1.07	1.08
MC LP (1) O3′ → σ* O4′H4′	1.00	0.78	1.04	1.03
PC LP (1) O3′ → σ* O4′H4′	1.00	0.77	1.02	1.02
KAPE LP (1) O3′ → σ* O4′H4′	1.01	0.78	1.03	1.02

(O)$H_{3'}\cdots O_{2'/4'}(CH_3)$ for both FA and FEA arenes (Fig. 1 and Supplementary Fig. 1). However, the impact of the mentioned stabilizing contacts was small. To investigate more precisely the nature of bond formation we carried out the NBO analysis at the M05-2X/6-311++G(d,p) level of theory. The results of donor–acceptor interactions and second-order perturbation energy *E*(2) [30] calculations are presented in Table 1. The interactions between the first lone pair of the oxygen and the O–H antibonding (σ*) orbital are related to calculated *E*(2) values (Table 1). On this account, it can be concluded that formed hydrogen bonds seem to be characterized by their low estimated energy values excluding CHLA derivatives (Table 1), which require further individual analysis (data not shown).

3.2. Bond dissociation enthalpy

BDE is the descriptor related to HAT mechanism (Eqs. 2.1 and 2.2). This is one of the most commonly studied approaches that describe thermodynamic stability of OH bond. The BDE parameter also characterizes the susceptibility of molecule to homolytic fission. It is well known that the lower the BDE is the more active is the OH moiety within the analyte. The general trends of ΔBDE_H and ΔBDE_G parameters (defined as a difference between BDE value of phenol and BDE value calculated for investigated compound) are given in Fig. 2 and Supplementary Fig. 2A. In this case, we used phenol as a standard to confirm the reliability of our calculations. Compounds were ordered based on the relation from highest to lowest ΔBDE values and were compared with phenol.

The estimated BDE data were in excellent agreement with experimental ones [31–36]. In general, we observed an interesting tendency, in case of most investigated compounds (from the PC-3′-OH to *c*-CHA-20′-OH derivatives given in Fig. 2 and Supplementary Fig. 2A) the most negative ΔBDE values were related to gaseous environment used for calculations. On the other hand, the most positive ΔBDE values corresponded to the previously mentioned analytes in water used as a solvent. It is in agreement with the fact that HAT mechanism is not preferred in this medium for the considered class of compounds [16,23]. Moreover, we observed higher antioxidant activity of esters (PC, KAPE, and MC) in comparison with corresponding acidic analogs with caffeic moiety (Fig. 2 and Supplementary Fig. 2A). The *t*-KA derivative, however, turned out to be weaker than its analogs discussed in this report (PC, KAPE, MC, *t*-DA, and *t*-NA). It was additionally found that *trans* isomers in gaseous phase indicated stronger antioxidant activity than corresponding *cis* isomers (the only exception was *t*-RA (16′-OH) derivative). We did not observe this tendency in SMD model using benzene or amyl acetate as solvents. In the molecule of *t*-RA with two phenyl rings and functional groups in the *ortho* position within all solvents used for calculations we observed that 3′-OH group in caffeic moiety was more susceptible to free radical attack. On the contrary, the *c*-RA derivative may be characterized by reverse dependence (16′-OH analog was more active than corresponding 3′-OH analog). We did not detect similar tendency for *t*-CHA and *c*-CHA analytes because within these arenes both phenyl rings with hydroxyl groups in the *para* position were associated with caffeic moiety. Furthermore, in both benzene and ethyl acetate media used for calculations as solvents the activity of three antioxidants (*c*-COA, *t*-COA, and *t*-*p*-CA as monohydroxy cinnamic acid derivatives) seem to be weakest unlike in case of other studied compounds. Therefore, we make an assumption that functional group in the *ortho* position influenced profitably on antioxidant activity and decreased BDE values of tested compounds.

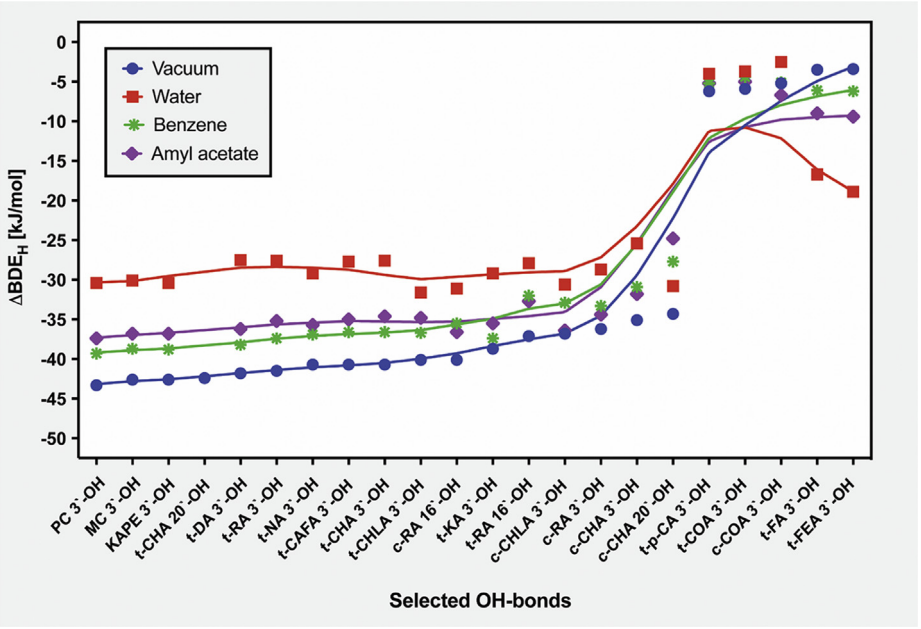

Fig. 2. Graphical representation of ΔBDE_H (kJ/mol) values calculated with M05-2X/6-311++G(d,p) level of theory. ΔBDE_H (kJ/mol) trend lines were calculated using LOWESS smoothing (locally weighted scatterplot smoothing) in GraphPad Prism 7.0a.

3.3. Proton affinity

The PA descriptor is an antioxidant factor related to a two-step SPLET mechanism (Eqs. 2.3 and 2.4). It describes susceptibility to heterolytic fission and thermodynamic stability of O—H bond. It is well known that the lower the PA value, the more stable is the studied compound [15,16]. The ΔPA_H and ΔPA_G values as descriptors related to the differences between the values of PA of phenol and PA of investigated molecule are presented in Fig. 3 and Supplementary Fig. 2B.

The corresponding results were in good agreement with the experimental data [37,38]. Taking into account the chemical environment used for the estimation

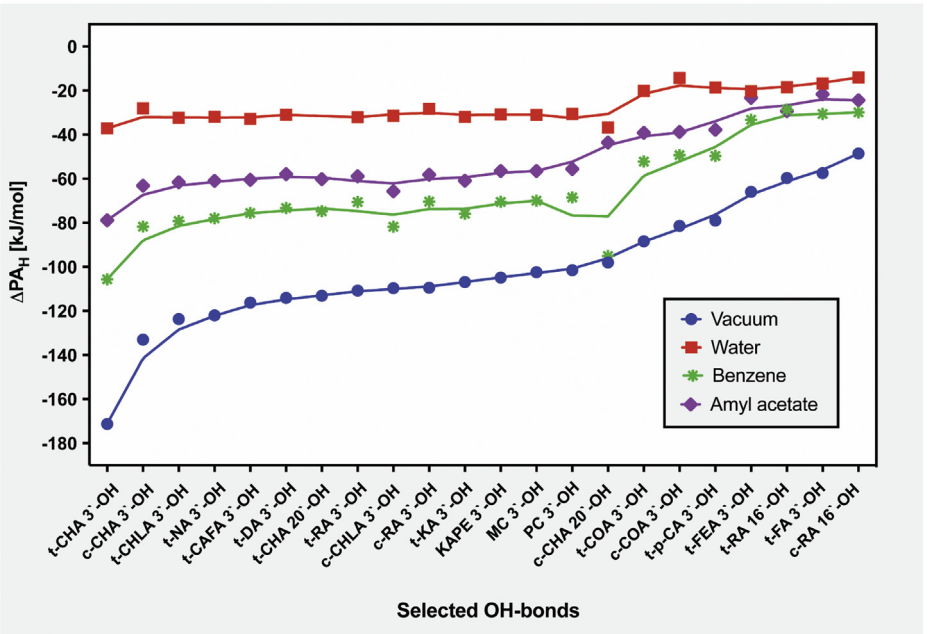

Fig. 3. Graphical representation of ΔPA_H (kJ/mol) values calculated with M05-2X/6-311++G(d,p) level of theory. ΔPA_H (kJ/mol) trend lines were calculated using LOWESS smoothing in GraphPad Prism 7.0a.

of ΔPA_H and ΔPA_G values for investigated arenes, we observed the fact that values of ΔPA were more negative when gaseous phase was considered and more positive in case of water used as a solvent (Fig. 3 and Supplementary Fig. 2B). Thus, gaseous phase turned out to be less favorable for proton donation. The PA_H values estimated *in vacuo* or in benzene and amyl acetate used for calculations as solvents for all studied compounds were much higher than the corresponding BDE_H values. Therefore, the SPLET mechanism seems to be less feasible in nonpolar and moderate polar media. On the contrary, the data calculated in water environment, in which PA_H values were much lower than corresponding BDE_H values, make SPLET approach privileged in polar media. The previously mentioned results led us to a conclusion that both isomers of chicoric acid were more active in polar media, unlike the corresponding ester derivatives (for which we observed reduction in activity in a nonpolar environment). Moreover, in nonpolar media caffeic acid did not turn out to be a leader of antioxidant activity among selected compounds. In all studied arenes, we observed that 3′-O–H group seems to be more proton-donating functionality than respective 4′-O–H (with exception of the *c*-CHA 4′-O–H derivative). Moreover, the O–H groups attached to the caffeic moiety in both isomers of RA could be characterized by better proton-donating abilities than respective O–H groups of 3,4-dihydroxyphenyl moieties. In the exception of two cases, namely, *c*-CHA 4′-O–H and *c*-CHA 20′O–H derivatives, *trans* isomers indicated higher activity than corresponding *cis* isomers. Considering the previously discussed HAT mechanism and results of PA calculations, we noticed that *ortho* position influenced significantly on antioxidant activity of analyzed compounds and loss of their PA values.

3.4. Adiabatic ionization potential

The AIP parameter is a numerical descriptor related to SET-PT mechanism (Eqs. 2.5 and 2.6). It describes the ability of the molecule to proton donation. Because the radicals with unpaired electrons within the structure of polyphenols were main reactants in antioxidant reactions, compounds with lower AIP were more active according to the mentioned mechanism [16,17,20,21]. The relationship between the estimated values of ΔAIP for investigated compounds and chemical environment considered for computations was very similar to the tendency noticed for estimation of ΔBDE and ΔPA values (Fig. 4 and Supplementary Fig. 2C). Moreover, as the values of AIP were much higher than respective BDE and PA (data not shown), the SET-PT mechanism was supposed not to be preferred for discussed library of molecules in nonpolar or polar media and therefore was not analyzed in details in our report.

3.5. Deprotonation energies

As was mentioned before free radicals' formation is also related to Fenton reaction catalyzed by transition metals in their reduced states, for example, Cu^+ and Fe^{2+}[17]. Moreover, hydroxyl, methoxyl, and carboxyl groups in phenolic compounds are known as a source of chelating moieties. The TMC mechanism (Eqs. 2.7 and 2.8) is related to the ability of analyte to create metal–ligand complexes. The most favorable chelation centers are connected to deprotonated hydroxyls. Metal chelating abilities can be measured quantitatively based on the acidity values ($\Delta H_{acidity}$ parameter estimated *in vacuo* and $\Delta G_{acidity}$ factor in media). The calculated difference between phenol data and investigated molecule ($\Delta\Delta H_{acidity}$ and $\Delta\Delta G_{acidity}$) is given in

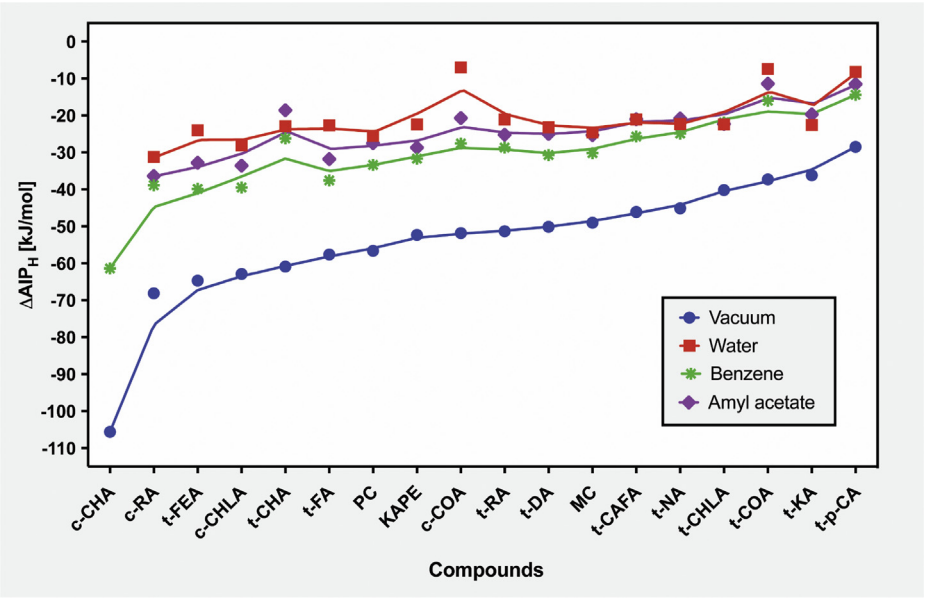

Fig. 4. Graphical representation of ΔAIP_H (kJ/mol) values calculated with M05-2X/6-311++G(d,p) level of theory. ΔAIP_H (kJ/mol) trend lines were calculated using LOWESS smoothing in GraphPad Prism 7.0a.

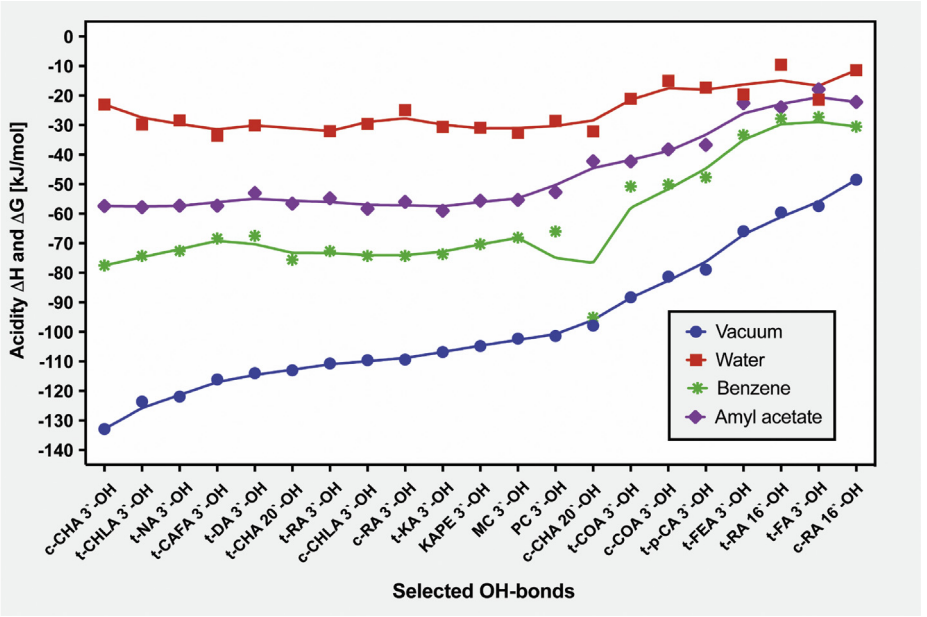

Fig. 5. Graphical representation of acidity values measured in vacuum as Δ*H* (kJ/mol) and in other media as Δ*G* (kJ/mol), calculated with M05-2X/6-311++G(d,p) level of theory. Δ*H* and Δ*G* (kJ/mol) trend lines were calculated using LOWESS smoothing in GraphPad Prism 7.0a.

Fig. 5. Acidity of all studied compounds turned out to be lower (when compared with phenol) in cases where only one O–H bond was considered. Moreover, *trans* isomers indicated lower values of energy deprotonation in the *para* position than respective *cis* isomers for all studied compound. The chelating leader among all studied *in vacuo* compounds turned out to be the *t*-CHA derivative being deprotonated in the *para* position. In all SMD model solvents it turned out that the greater chelating ability was related to PC 4′-O–H, *c*-CHA 3′-O–H, and *c*-RA 16′-O–H derivatives. However, it has to be noticed that the values of energy deprotonation were highly adjacent and therefore should not be treated as the primary determinant.

3.6. Stabilization energies (ΔE_{ISO})

Determination of stabilization energies is a simple theoretical method, which helps to determine the scavenging ability of the molecule [39]. It is related to the free radicals generated via the HAT mechanism. The ΔE_{ISO} parameters (Eqs. 2.9 and 2.10) were estimated according to the reactions between the DPPH and phenol radicals (Table 2; reactions 3.6.1. and 3.6.2.). Moreover, it is noteworthy that the calculation of ΔE_{ISO} values might be useful tool for the prediction of stability of functional groups [16].

$$ArOH + DPPH \rightarrow ArO^{\bullet} + DPPHH \quad (3.6.1.)$$

Table 2
ΔE_{ISO} (kJ/mol) calculated with M05-2X/6-311++G(d,p) in vacuum, water, benzene, and amyl acetate.

Bond	ΔE_{ISO} with DPPH				ΔE_{ISO} with phenol radical			
	Vacuum	Water	Benzene	Amyl acetate	Vacuum	Water	Benzene	Amyl acetate
Phenol	41.9	36.1	36.4	35.0	0.0	0.0	0.0	0.0
t-FA 3′-O–H	38.5	15.7	29.6	25.1	−3.4	−20.4	−6.8	−9.9
t-KA 3′-O–H	1.5	5.5	−3.2	−2.6	−40.4	−30.5	−39.6	−37.6
t-*p*-CA 3′-O–H	36.1	31.9	31.0	29.8	−5.8	−4.2	−5.3	−5.3
c-CHLA 3′-O–H	3.2	4.8	1.5	−2.1	−38.6	−31.3	−35.0	−37.2
t-CHLA 3′-O–H	−0.2	5.5	−2.3	−2.2	−42.1	−30.5	−38.7	−37.2
t-NA 3′-O–H	−0.4	5.5	−2.4	−2.1	−42.3	−30.6	−38.8	−37.1
c-RA 3′-O–H	3.7	5.8	−0.5	−1.1	−38.2	−30.3	−36.9	−36.1
t-RA 3′-O–H	−1.9	6.0	−3.5	−2.8	−43.8	−30.0	−39.9	−37.9
c-COA 3′-O–H	38.6	33.2	32.7	30.2	−3.2	−2.8	−3.7	−4.8
t-COA 3′-O–H	36.3	33.1	31.6	30.6	−5.6	−3.0	−4.8	−4.5
t-CAFA 3′-O–H	−1.1	6.3	−2.9	−2.2	−43.0	−29.6	−39.3	−37.2
t-FEA 3′-O–H	38.6	16.3	29.6	25.2	−3.3	−19.8	−6.8	−9.8
t-DA 3′-O–H	−2.0	6.2	−3.9	−3.3	−43.9	−29.9	−40.3	−38.3
c-CHA 3′-O–H	5.9	8.8	4.0	4.4	−36.0	−27.2	−32.4	−30.6
t-CHA 3′-O–H	−1.0	6.5	−2.8	−2.2	−42.9	−29.6	−39.2	−37.2
MC 3′-O–H	−2.8	4.7	−4.4	−3.8	−44.7	−31.4	−40.8	−38.8
PC 3′-O–H	−3.5	4.6	−5.1	−4.3	−45.4	−31.5	−41.5	−39.3
KAPE 3′-O–H	−3.0	4.9	−4.6	−3.9	−44.8	−31.1	−40.9	−38.9

$$ArOH + PhO^{\bullet} \rightarrow ArO^{\bullet} + PhOH \quad (3.6.2.)$$

Because it was proved in our previous investigations that the presence of hydroxyl group in the *para* or *ortho* position had stronger influence on antioxidant's stability than the *meta* position, we focused only on 3′-O—H bond [16]. The lowest stabilization energy values were recorded for esters (PC, KAPE, and MC derivatives), whereas the highest values were observed in case of monohydroxy derivatives (*t*-*p*-CA, *t*-COA, and *c*-COA). Our results concurred with previously observed phenomenon [16], in which the contribution of *o*-O atom very effectively stabilized the structure of free radical being responsible for the antioxidant activity of analyzed compounds.

3.7. HOMO and LUMO—distribution and energy

The HOMO and LUMO are meaningful indicators of the molecular electron structure. High energy of LUMO (E_{LUMO}) value is related to good electron donating abilities, whereas low energy of HOMO (E_{HOMO}) value corresponds to weak electron donation. Moreover, distribution of the frontier molecular orbitals is essential in the analysis of antioxidant potential and can indicate the active moieties susceptible for free radical attack. In our study, we observed the lowest energy gaps between HOMO and LUMO *in vacuo* for *c*-RA, *c*-CHA, and *t*-CHA derivatives, which indicated that these compounds are supposed to be potentially characterized by faster electron transition from ground to excited state. Graphical representation illustrating this phenomenon is depicted in Supplementary Fig. 3 for vacuum. Furthermore, as support for graphical representation the $\Delta E(E_{LUMO} - E_{HOMO})$ values for all media have been calculated and summarized in Table 3.

Detailed analysis of these data indicated that the ΔE values were similar for both *cis* and *trans* isomers in gaseous phase and all studied media. Moreover, the resulted data revealed that caffeic acid derivatives were characterized by very good electron donating abilities.

We also observed that the electron density of HOMO was localized on the benzene ring and vinyl bond in all of the investigated molecules. The presence of hydroxyl group in the *para* position (*t*-*p*-CA, *t*-COA, *c*-COA, and *t*-FA derivatives) and *o*-dihydroxy substitution contributed to the HOMO distribution within their structure. The electron density of LUMO was concentrated on the C_6—C_7 and C_8—C_9 bonds together with respective C_{14}—C_{15} and C_{16}—C_{17} bonds (*c*-CHA and *t*-CHA derivatives), as well as C-2, C-4, and C-6 carbon atoms in the phenyl ring. On the other hand, the spectral effect caused by hydroxylation of the phenyl ring in the *meta* position was not observed despite its contribution to the HOMO plot. However, the whole molecules of analyzed arenes participated in the electron transition from ground to excited state. Albeit the delocalization of the electron density positively influenced on molecular stabilization of analytes, O-atom located in the *para* position seems to be the most active region in caffeic acid derivatives.

3.8. SD and SOMO distribution of radicals

In accordance with HAT, SPLET, and SET-PT mechanisms, hydroxyl radicals of all investigated molecules were final products caused by the influence of free radicals. Distribution of SOMOs showed the resonance structure formation of the studied radicals obtained by elimination of the hydrogen atom from the hydroxyl group (data not shown). We supported discussion about the resonance geometries of analytes by calculation of their total SD values. The graphical presentation of resulted data is given in Supplementary Fig. 4. On the basis of the SOMO analysis, it was observed that unpaired electron was delocalized on O-atom, phenyl ring, and vinyl bond. These patterns remain constant for *cis* and *trans* isomers and in all studied media. Considering calculated SD values (calculations carried out in vacuum), we observed that the phenoxy group had the

Table 3
E_{HOMO}, E_{LUMO}, and $\Delta E(E_{LUMO} - E_{HOMO})$ calculated with rM05-2X/6-311++G(d,p) in vacuum, water, benzene, and amyl acetate.

Compound	Water			Benzene			Amyl acetate		
	E_{HOMO} (eV)	E_{LUMO} (eV)	ΔE (eV)	E_{HOMO} (eV)	E_{LUMO} (eV)	ΔE (eV)	E_{HOMO} (eV)	E_{LUMO} (eV)	ΔE (eV)
Phenol	−7.9	0.5	8.4	−7.8	0.6	8.4	−7.8	0.5	8.3
t-FA	−7.4	−1.1	6.3	−7.4	−1.0	6.4	−7.4	−1.0	6.4
t-KA	−7.5	−1.1	6.4	−7.5	−1.0	6.5	−7.5	−1.0	6.5
t-*p*-CA	−7.6	−1.1	6.5	−7.6	−1.0	6.6	−7.6	−1.0	6.6
c-CHLA	−7.5	−1.0	6.5	−7.5	−1.0	6.5	−7.5	−1.0	6.5
t-CHLA	−7.5	−1.1	6.4	−7.6	−1.1	6.5	−7.5	−1.0	6.5
t-NA	−7.5	−1.1	6.4	−7.5	−1.0	6.5	−7.5	−1.0	6.5
c-RA	−7.5	−1.0	6.5	−7.4	−1.1	6.3	−7.4	−0.9	6.5
t-RA	−7.5	−1.2	6.3	−7.5	−1.0	6.5	−7.5	−1.0	6.5
c-COA	−7.7	−1.0	6.7	−7.6	−1.0	6.6	−7.6	−1.1	6.5
t-COA	−7.6	−1.2	6.4	−7.6	−1.0	6.6	−7.6	−1.0	6.6
t-CAFA	−7.5	−1.2	6.3	−7.5	−1.1	6.4	−7.5	−1.1	6.4
t-FEA	−7.4	−1.2	6.2	−7.4	−1.0	6.4	−7.4	−1.0	6.4
t-DA	−7.5	−1.1	6.4	−7.5	−1.0	6.5	−7.4	−1.0	6.4
c-CHA	−7.5	−1.2	6.3	−7.4	−1.0	6.4	−7.4	−1.1	6.3
t-CHA	−7.5	−1.3	6.2	−7.5	−1.1	6.4	−7.4	−1.1	6.3
MC	−7.5	−1.0	6.5	−7.4	−0.9	6.5	−7.4	−0.9	6.5
PC	−7.5	−1.0	6.5	−7.4	−0.8	6.6	−7.4	−0.9	6.5
KAPE	−7.5	−1.0	6.5	−7.4	−0.9	6.5	−7.4	−0.9	6.5

Table 4
SD values calculated with uM05-2X/6-311++G(d,p) in vacuum describing input to SOMOs of the following groups: phenoxy group, phenyl ring, C_7–C_8, and C_{15}–C_{16} bond.

Compound	Phenoxy group	Phenyl ring	C_7–C_8 bond	C_{15}–C_{16} bond
t-FA	0.35	0.62	0.18–0.37	n/a
t-KA	0.36	0.20	0.21–0.20	n/a
t-*p*-CA	0.39	0.20	0.26–0.39	n/a
c-CHLA	0.36	0.26	0.21–0.28	n/a
t-CHLA	0.36	0.04	0.29–0.22	n/a
t-NA	0.36	0.01	0.29–0.20	n/a
3′-O-*c*-RA	0.36	0.42	0.23–0.32	n/a
16′-O-*c*-RA	0.42	1.27	0.02–0.00	n/a
3′-O-*t*-RA	0.36	0.09	0.24–0.20	n/a
16′-O-*t*-RA	0.42	1.15	0.29–0.02	n/a
c-COA	0.41	0.78	1.63–2.70	n/a
t-COA	0.38	0.07	0.23–0.27	n/a
t-CAFA	0.36	0.06	0.28–0.18	n/a
t-FEA	0.35	0.55	0.23–0.23	n/a
t-DA	0.36	0.06	0.27–0.19	n/a
3′-O-*c*-CHA	0.38	1.10	0.09–0.20	0.02–0.06
20′-O-*c*-CHA	0.36	2.72	1.29–0.02	0.40–0.60
3′-O-*t*-CHA	0.36	0.01	0.28–0.20	0.03–0.12
20′-O-*t*-CHA	0.36	0.25	0.23–0.01	0.18–0.17
MC	0.36	0.29	0.21–0.25	n/a
PC	0.36	0.17	0.24–0.22	n/a
KAPE	0.36	0.15	0.26–0.22	n/a

largest contribution to SOMO within the structure of analyzed compounds (Table 4). The total contribution to SOMO of the phenyl ring and the impact on SOMOs influenced by the C_7–C_8 bond are also presented in Table 4. Moreover, the SOMO distribution in case of 16′-O-*t*-RA and 16′-O-*c*-RA derivatives (SOMOs located only in plane of the phenyl ring) leads to a decrease in radical stability.

4. Conclusion

We have carefully analyzed the library of caffeic acid derivatives, regarding their antioxidant activity and determined descriptors as a continuation of our recently published results on this account. The ferulic, *p*-coumaric, chlorogenic, and caffeic acids were recently investigated; however, there are no data computations on antioxidant activity of fertaric, coutaric, caftaric, dactylifric, neochlorogenic acids and PC. Therefore, on this account to fill this gap the presented study is the first attempt to investigate their antioxidant activity using *in silico* techniques. For this purpose, we focused our attention on HAT, SPLET, SET-PT, and TMC mechanisms to be possible to occur, determining concurrently several parameters such as BDE, PA, AIP, HOMO, LUMO, SOMO, SD, ΔE_{ISO}, $\Delta H_{acidity}$, and $\Delta G_{acidity}$, as well as $E(2)$ (NBO).

Herein, however, we extended our studies on compounds' "behavior" in benzene and amyl acetate media to simulate the hydrophobic environment of the plasma membrane.

In case of most investigated compounds the most negative ΔBDE, ΔPA, and ΔAIP values were related to the gaseous environment used for calculations. On the other hand, their most positive values corresponded to the analytes in water used as a solvent. Furthermore, the lowest stabilization energy values were recorded for esters (PC, KAPE, and MC derivatives), whereas the highest ones were observed in case of monohydroxy derivatives (*t*-*p*-CA, *t*-COA, and *c*-COA). Our investigations allowed us to make an assumption that the most active antioxidants (according to the HAT approach) were compounds PC, MC, and KAPE, whereas the activity of *t*-CHA and *c*-CHA derivatives was related to the SPLET protocol. We observed that well described in the literature lead compounds (*t*-KA, *t*-FA, and *t*-*p*-CA) appeared not to be top effective when compared with other studied caffeic acid derivatives. Moreover, we have noticed that the *ortho* position influenced profitably antioxidant activity in all analyzed compounds.

We also observed that the estimated ΔE ($E_{LUMO} - E_{HOMO}$) values were similar for both *cis* and *trans* isomers of investigated compounds in the gaseous phase and all studied media. On this account caffeic acid derivatives were characterized by very good electron donating abilities.

Involving the SOMO analysis, we noticed that unpaired electron was delocalized on O-atom, phenyl ring, and vinyl bond within the structure of analyzed derivatives (*cis* and *trans* isomers and in all media used for calculations). Moreover, considering calculated SD values (calculations carried out in vacuum), we observed that the phenoxy group had the largest contribution to SOMO within the structure of analyzed arenes.

The resulted data involving DFT formalism and SMD solvation model make final conclusion that our proposed methodology seems to be a useful tool for prediction antioxidant activity of caffeic acid derivatives. The proposed assumption will be carefully investigated by our group in the near future.

Acknowledgments

This study was supported by Poznan Supercomputing and Networking Center (PCSS) grant no. 164 entitled "Theoretical study of antioxidant properties of ester derivatives of resveratrol and cinnamic acids" (A.U.). This research was also supported in part by the PL-Grid Infrastructure and the Wroclaw Center for Networking and Supercomputing (WCSS grant No. 327/2014) grants. The authors are thankful to Prof. Karol Kacprzak for his valuable suggestions regarding this manuscript.

Authors contribution: A.U. contributed to performance of calculations, initial results interpretation, support in experiments design and manuscript preparation, K.C. supported in the manuscript preparation, J.K. corrected the manuscript, and M.S. participated in manuscript preparation, experiments design, results interpretation, final conclusions statement, project supervision and was idea holder.

Appendix A. Supplementary data

Supplementary data related to this article can be found at http://dx.doi.org/10.1016/j.crci.2017.08.003.

References

[1] K. Apel, H. Hirt, Annu. Rev. Plant Biol. 55 (2004) 373–399.

[2] C. Manach, A. Scalbert, C. Morand, C. Rémésy, L. Jiménez, Am. J. Clin. Nutr. 79 (2004) 727.
[3] K.L. Johnston, M.N. Clifford, L.M. Morgan, Am. J. Clin. Nutr. 78 (2003) 728–733.
[4] F. Natella, M. Nardini, I. Giannetti, C. Dattilo, C. Scaccini, J. Agric. Food Chem. 50 (2002) 6211–6216.
[5] J.P. Spencer, M.M.A. El Mohsen, A. Minihane, J.C. Mathers, Br. J. Nutr. 99 (2008) 12–22.
[6] I. Gulçin, Toxicology 217 (2006) 213–220.
[7] L. Zhang, Z. Wang, W. Zhang, Chinese J. Chromatogr. 31 (2013) 122–126.
[8] V.L. Singleton, J. Zaya, E.K. Trousdale, Phytochemistry 25 (1986) 2127–2133.
[9] X. Zhang, R. Ishida, Y. Yuhara, T. Kamiya, T. Hatano, G. Okamoto, S. Arimoto-Kobayashi, Mutat. Res. – Genet. Toxicol. Environ. Mutagen. 723 (2011) 182–189.
[10] M. Villarino, P. Sandín-España, P. Melgarejo, A. De Cal, J. Agric. Food Chem. 59 (2011) 3205–3213.
[11] S.U. Chon, Curr. Pharm. Des. 19 (2013) 6112–6124.
[12] G. Wang, Z. Lei, Q. Zhong, W. Wu, H. Zhang, T. Min, H. Wu, F. Lai, Food Chem. 15 (2017) 332–341.
[13] P. Maisuthisakul, R. Pongsawatmanit, M.H. Gordon, J. Agric. Food Chem. 54 (2006) 2719–2725.
[14] P. Maisuthisakul, R. Pongsawatmanit, M.H. Gordon, Food Chem. 100 (2007) 1620–1629.
[15] E.G. Bakalbassis, N. Nenadis, M. Tsimidou, J. Am. Oil Chem. Soc. 80 (2003) 459.
[16] M. Szeląg, A. Urbaniak, H.A.R. Blyussen, Open Chem. 13 (2015) 17–31.
[17] M. Leopoldini, N. Russo, M. Toscano, Food Chem. 125 (2011) 288–306.
[18] M.C. Foti, C. Daquino, C. Geraci, J. Org. Chem. 69 (2004) 2309–2314.
[19] G. Litwinienko, K.U. Ingold, Acc. Chem. Res. 40 (2007) 222–230.
[20] M. Szeląg, D. Mikulski, M. Molski, J. Mol. Model. 18 (2012) 2907–2916.
[21] J. Rimarcik, V. Lukes, E. Klein, M. Ilcin, J. Mol. Struct. THEOCHEM 952 (2010) 25–30.
[22] M. Leopoldini, N. Russo, M. Toscano, J. Agric. Food Chem. 54 (2006) 3078–3085.
[23] S. Sebastian, N. Sundaraganesan, S. Manoharan, Spectrochim. Acta, Part A 74 (2009) 312–323.
[24] Y. Zhao, N.E. Schultz, D.G. Truhlar, J. Chem. Theory Comput. 2 (2006) 364–382.
[25] O. Holtomo, M. Nsangou, J.J. Fifen, O. Motapon, J. Mol. Model. 20 (2014) 2509.
[26] G.M. Sulaiman, A.A. Al-Amiery, R. Bagnati, Int. J. Food Sci. Nutr. 65 (2014) 101–105.
[27] H. Cao, W.X. Cheng, C. Li, X.L. Pan, X.G. Xie, T.H. Li, J. Mol. Struct. THEOCHEM 719 (2005) 177–183.
[28] G. Mariappan, N. Sundaraganesan, S. Manoharan, Spectrochim. Acta, Part A Mol. Biomol. Spectrosc. 97 (2012) 340–351.
[29] M. Saqib, S. Iqbal, A. Mahmood, R. Akram, Int. J. Food Prop. 19 (2016) 745–751.
[30] G.A. Jeffery, in: Introduction to Hydrogen Bonding, Oxford University Press, New York, 1997.
[31] P. Mulder, O.W. Saastad, D. Griller, J. Am. Chem. Soc. 110 (1988) 4090–4092.
[32] A.J. Colussi, F. Zabel, S.W. Benson, Int. J. Chem. Kinet. 9 (1977) 161–178.
[33] D.J. DeFrees, R.J. McIver Jr., W.J. Hehre, J. Am. Chem. Soc. 102 (1980) 3334.
[34] J.A. Walker, W. Tsang, J. Phys. Chem. 94 (1990) 3324.
[35] I.W.C.E. Arends, R. Louw, P.J. Mulder, J. Phys. Chem. 97 (1993) 7914–7925.
[36] J. Lind, X. Shen, T.E. Eriksen, G. Merenyi, J. Am. Chem. Soc. 112 (1990) 479.
[37] M. Fujio, R.T. McIver, R.W. Taft, J. Am. Chem. Soc. 103 (1981) 4017–4029.
[38] T.B. McMahon, P. Kebarle, J. Am. Chem. Soc. 99 (1977) 2222.
[39] A.N. Queiroz, B.A.Q. Gomes, W.M. Moraes Jr., R.S. Borges, Eur. J. Med. Chem. 44 (2009) 1644–1649.
[40] Gaussian 09, Revision A.02, M.J. Frisch, G.W. Trucks, H. B. Schlegel, G.E. Scuseria, M.A. Robb, J.R. Cheeseman, G. Scalmani, V. Barone, G.A. Petersson, H. Nakatsuji, X. Li, M. Caricato, A. Marenich, J. Bloino, B.G. Janesko, R. Gomperts, B. Mennucci, H.P. Hratchian, J.V. Ortiz, A.F. Izmaylov, J.L. Sonnenberg, D. Williams-Young, F. Ding, F. Lipparini, F. Egidi, J. Goings, B. Peng, A. Petrone, T. Henderson, D. Ranasinghe, V.G. Zakrzewski, J. Gao, N. Rega, G. Zheng, W. Liang, M. Hada, M. Ehara, K. Toyota, R. Fukuda, J. Hasegawa, M. Ishida, T. Nakajima, Y. Honda, O. Kitao, H. Nakai, T. Vreven, K. Throssell, J.A. Montgomery, Jr, J.E. Peralta, F. Ogliaro, M. Bearpark, J.J. Heyd, E. Brothers, K.N. Kudin, V.N. Staroverov, T. Keith, R. Kobayashi, J. Normand, K. Raghavachari, A. Rendell, J. C. Burant, S.S. Iyengar, J. Tomasi, M. Cossi, J.M. Millam, M. Klene, C. Adamo, R. Cammi, J.W. Ochterski, R.L. Martin, K. Morokuma, O. Farkas, J.B. Foresman, D.J. Fox, Gaussian, Inc., Wallingford CT, 2016.
[41] Y. Zhao, D.G. Truhlar, J. Chem. Theory Comput. 3 (2007) 289–300.
[42] A.V. Marenich, C. Cramer, D.G. Truhlar, J. Phys. Chem. B 113 (2009) 6378–6396.
[43] P.W. Atkins, Physical Chemistry, sixth ed., Oxford University Press, Oxford, 1998.
[44] V.D. Parker, J. Am. Chem. Soc. 114 (1992) 7458.
[45] M.M. Bizarro, B.J.C. Cabral, R.M.B. dos Santos, J.A.M. Simões, Pure Appl. Chem. 71 (1999) 1249–1256.